Advances in Aircraft and Spacecraft Science, *Vol. 6, No. 4 (2019) 283-296*
DOI: https://doi.org/10.12989/aas.2019.6.4.283

Trailing edge geometry effect on the aerodynamics of low-speed BWB aerial vehicles

Mohammed A. Ba Zuhair*

Department of Aerohydrodynamics, Kazan National Research Technical University - KAI, Kazan, Karl Marx 10, Russian Federation

(Received December 6, 2018, Revised January 28, 2019, Accepted January 29, 2019)

Abstract. The influence of different planform parameters on the aerodynamic performance of large-scale subsonic and transonic Blended Wing Body (BWB) aircraft have gained comprehensive research in the recent years, however, it is not the case for small-size low subsonic speed Unmanned Aerial Vehicles (UAVs). The present work numerically investigates aerodynamics governing four different trailing edge geometries characterizing BWB configurations in standard flight conditions at angles of attack from -4° to 22° to provide generic information that can be essential for making well-informed decisions during BWB UAV conceptual design phase. Simulation results are discussed and comparatively analyzed with useful implications for formulation of proper mission profile specific to every BWB configuration.

Keywords: flying wing; BWB; BWB aerodynamic design; low-speed aerodynamics; wing planform

1. Introduction

The growing demand over the last two decades toward realizing environmentally-friendly aviation notably drove aerodynamic designers to refresh research and development works on the potential of fuel efficient, quiet and more capable solutions derived from Flying Wing (FW) concepts. The main interest hitherto is focusing on Hybrid Wing Body (HWB) or Blended Wing Body (BWB) unconventional configurations. The key distinguishing factor between FW and BWB concepts is represented in the degree of fuselage/wing geometrical blending, where BWB is characterized by evident wing planform and fuselage boundaries (Okonkwo, P., & Smith, H., 2016). Such an interest is motivated by the observed improvement of commercial subsonic and transonic technical performance achievable as a result of the transition from tube-and-wing aircraft configuration to BWB. Comparative analysis of the latter versus conventional aircraft designs conducted by (Liebeck 2004, Kroo 2004, Qin *et al.* 2004) demonstrated superior aerodynamic performance such as skin friction drag reduction due to the decrease of wetted area enabling higher lift-to-drag ratios. From an aeroelastic standpoint, the all-lifting design reduces the wing spanwise loading thanks to the contribution of centerbody structural elements, which also improves lift distribution as a result of minimized flow interference and wave drag at high subsonic and transonic speeds. Absence of vertical stabilizer substantially reduces weight and total drag

*Corresponding author, Ph.D. Student, E-mail: mohammed-ba@yandex.ru

http://www.techno-press.org/?journal=aas&subpage=7 ISSN: 2287-528X (Print), 2287-5271 (Online)

penalties at the tail section providing laminar flow zone to be exploited by additional active flow control devices and powerplants. Moreover, it has been established that mounting engines properly within the aft part of the centerbody of BWB aircraft results in ram drag reductions utilizing Boundary Layer Ingestion (BLI) (Kawai *et al.* 2006). Removed engine pylons and smaller nacelle surface area also benefit aerodynamic performance and flight dynamics. Buried engines in the airframe improve pitching controllability, when pylons are being eliminated, and thrust reversers instead enjoy better positioning leading to the achievement of less aircraft weight and landing field distance (Geiselhart *et al.* 2003). Furthermore, trailing edge control surfaces efficiency and functionality may be considerably improved by turbulent flow immersing the horizontal stabilizer of a conventional aircraft at certain angles of attack, e.g., deep stall. This additionally allows the adoption of high multifunctional control surfaces for active control system (Okonkwo and Smith 2016) or even such as flaps and elevons working as airbrakes and control surfaces simultaneously (Ba Zuhair 2018). In fact, one of the advantageous geometrical properties of BWB configurations lies at the spanwise trailing edge in the sense that it helps considering a plenty of design options for effective trim control surfaces and flow control solutions.

The requirement to achieve high Mach numbers flights, nearly 0.8-1.3, for large transport aircraft predicates favoring sweptback wing planform designs. For FW and BWB configurations regardless of cruise speed prerequisites this becomes an inevitable design tradeoff for the sake of attaining desired stability and controllability. Therefore, modern leading edge sweep angles range from 30°-50° in average, since variable sweptback wings are widespread, while designs earlier than 1950s overcome the longitudinal stability and control difficulties by mounting horizontal stabilizers to small diameter fuselage-like structures as well as wingtip rudders for lateral control (Okonkwo *et al.* 2016 and Wood *et al.* 2011). Today, longitudinal and lateral trim and control is provided by the careful optimization of planform, airfoil stack, and twist distribution to instill a degree of inherent static stability of BWB at cruise modes with necessary intensive implementation of fly-by-wire technology and active control systems to handle unstable flight modes (Liebeck 2004 and Voskuijl *et al.* 2008). Effects of aspect ratio and high and/or variable leading edge sweep on the aerodynamic characteristics of FW and BWB large-scale aircraft have been richly investigated by Okonkwo *et al.* (2016), Liebeck (2004), Kroo (2004) and Qin *et al.* (2004) in addition to Siouris *et al.* (2007), Meheut *et al.* (2012) & Kuntawala (2011). The main goal of these studies was to understand flow compressibility effects in transonic conditions with particular focus on wave drag development, handling, and control instabilities in order to synthesize optimal design constraints. However, the appealing advantages of BWB concept are neither specific to high-capacity commercial transport aircraft nor even to military heavy payload delivery applications. The exponentially increasing interest in designing fast and small Unmanned Aerial Vehicles (UAVs) to fly at low Reynold's numbers occasionally stimulates more and more conceptualization and brainstorming works for creating innovative concepts one of which has become BWB for civilian and military UAVs.

Geometrical, operational, and physiological constraints stipulated by the nature of large BWB operation vanish in the design process of their low-speed unmanned versions. Centerbody design significantly simplified due to the absence of pressurized vessels to satisfy passenger cabin safety requirements which in result provides structural benefits, still not mentioning the technological ones. Issues of transonic drag, cockpit, and passenger cabin layout, passenger acceptance, ride quality, and emergency egress are consequently resolved.

Indeed, this is why a number of works to examine BWB geometry implementation for UAV applications started being actively conducted. A variety of parameterized BWB configurations was numerically studied by Panagiotou *et al.* (2017) to provide a preliminary insight for conceptual designers while selecting wing planform parameters with sufficient knowledge of their effects on lift and drag. Computer Aided Design (CAD) generated geometries with five design variants of sweep angles as follows: -10°, 0°, 20°, 40°, and conventional (low-taper straight wing with tail parts) were studied concluding the zero and highly sweptback wings superiority in terms of the aerodynamic performance. Another experimentally tested concept was discussed by Lehmkuehler (2012) for three-meters-span low-sweep wing UAV with twin vertical stabilizers. Additionally, detailed physical and numerical analysis for two BWB configurations: a typical BWB geometry, i.e., similar to baseline B-450 in (Liebeck 2004) with equilateral triangle-like trailing edge and a second design equipped with a pair of canards in front of its main wings was given in (Wisnoe *et al.* 2009, 2010). Similarly, it seems that although Shim and Park in (Smith *et al.* 2013) and Patel M. *et al.* (2007) investigated different BWB control issues, they both adopted almost analogical wing planform parameters for their studies but with different airfoil sections. All the aforementioned studies except (Panagiotou *et al.* 2017) described single models conceptualized based on the experience and intuition of their designers, while (Panagiotou *et al.* 2017) provides a generic parametric study for BWB leading edge sweep aerodynamics, which is generally unavoidable choice during the conceptual design decision making process for its well-known benefits on longitudinal stability and trim of FW-like aerial vehicles. On the other hand, trailing edge geometry may involve inconstant sweep. Basically, this can be preferred, sometimes required, for conceptualizing UAVs with high maneuverability and trim capabilities. However, literature review reveals that BWB configuration designers may suffer a lack of informative guidelines and aerodynamic studies in a concise reference on the potential benefits and penalties for answering what exact trailing edge scheme to be chosen.

Therefore, in this work an effort is made to provide amateur engineers and designers of small-size BWB UAVs with a generic reference on key aerodynamic effects caused by trailing edge geometry or sweep parameters so as to facilitate its well-informed and successful selection during BWB conceptual design studies.

2. Aerodynamic analysis methodology

In the majority of flying vehicle conceptualization works initial budget constraints require the consideration of alternative low-cost, mostly numerical, approaches to examine feasibility and performance of the innovated solutions. This becomes crucial for catching the first glimpse on the aerodynamics of various BWB designs especially for transonic flow regimes due to scarce real flight and experimental data or their proprietary nature (Voskuijl *et al.* 2008, Lehmkuehler 2012). More common practice is to employ repeatedly validated low- and high-fidelity CFD tools with validity and accuracy establishment based on the adequate setting of the selected boundary conditions, grid sensitivity, and turbulence models (Qin *et al.* 2004, Voskuijl *et al.* 2014, Siouris *et al.* 2007, Meheut *et al.* 2012, Kuntawala *et al.* 2011, Vicroy *et al.* 2009 and Panagiotou *et al.* 2017). In the case of low Mach speeds (M) within 0.05-0.3 easier testing apparatus and conditions facilitated performing few wind tunnel analyses for a variety of BWB configurations as in (Wisnoe *et al.* 2009, 2010, Shim *et al.* 2013, Patel *et al.* 2007 and Gursul 2004). Considering overall geometrical similarity of BWB, for example in (Patel *et al.* 2007, Gursul 2004, Higgins *et al.* 1928 and Spalart *et al.* 2007), some experimentally investigated configurations in the references can be

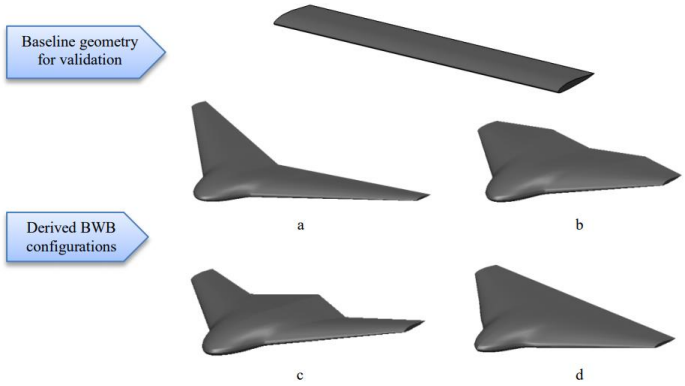

Fig. 1 Derived BWB configurations from baseline geometry

Table 1 Geometrical specifications of the investigated BWB configurations

	a	b	c	d
Leading edge sweep, deg.	45	45	45	45
Area, m^2	0.287	0.287	0.287	0.287
Wing span, m	0.78	0.56	0.64	0.59
Taper	0.177	0.195	0.19	0.195
Aspect ratio	4.36	2.3	2.9	2.5
Trailing edge sweep				
Root edge, deg.	22.25	+15	–30	0
Tip edge, deg.	22.25	+15	–25	0

utilized for low-fidelity comparative analysis and validation considering approximate boundary conditions.

2.1 Geometry generation

At the beginning 6-inch by 36-inch wing of the NACA-M6 airfoil section was generated by CAD tool SolidWorks 2016, merely for method validation, considering flap and aileron segmentation removal (Higgins *et al.* 1928). Using built-in measuring tools, overall reference (A_{ref}) and surface area (A_{sur}) were precisely calculated. To study only the effect of trailing edge properties without manipulating other geometrical parameters, especially A_{sur} because it may lay beyond the fundamental cause of aerodynamic performance variations within normalized boundary conditions, four other designs were derived as shown in Fig. 1 characterized by the same leading edge sweep (Λ) and nose geometry, all to satisfy BWB criteria of smooth fuselage/wing blending, in addition to preserving baseline model A_{sur} in order to restrict work concentration on planform effects particularly trailing edge (since A_{sur} increase will reflect on wetted area increase, weight, and structural penalties) and facilitating validation procedure.

Corresponding designs resulted in the following geometrical parameters listed in Table 1 for the same operational conditions: Reynold's number (Re) = 500000, standard weather conditions at sea level with 1.225 kg/m^3 atmospheric density, 101325 Pa atmospheric pressure, 26.8° temperature, zero wind magnitude and direction. The chosen fixed Re in this investigation satisfies

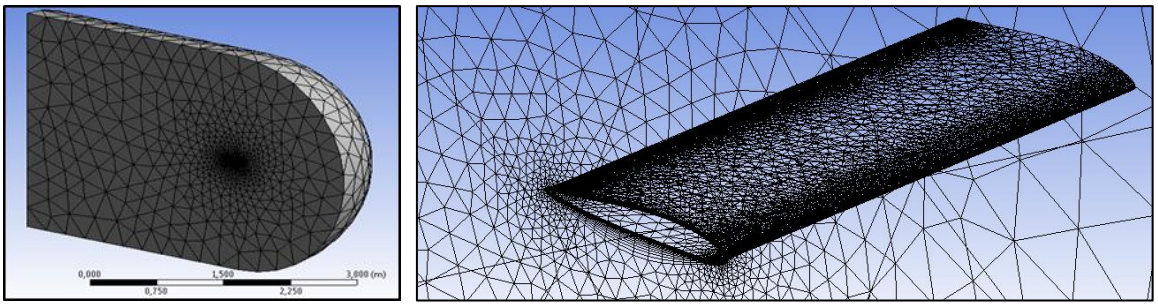

Fig. 2 Mesh around the simulated NACA-M6

flow turbulence properties at low subsonic flight achieved by the majority of current electrically powered UAVs.

2.2 Method validation

Based on that, this work imported baseline experimentally investigated finite span wing geometry generated from NACA-M6 (Higgins *et al.* 1928) airfoil featured by a zero pitching moment coefficient (C_m) at horizontal flight modes, i.e., zero angle of attack (α) to satisfy FW and BWB configuration requirements. In principle, these early tests were conducted to study aerodynamics concerning trailing edge control surfaces, namely flaps and ailerons, at average Re around 4.28 million. However, abundance of the accumulated data may be utilized reservedly as indicative validation data in other conceptual studies for flights at lower Re.

For task simplification and computation time acceleration purposes at conceptual design phase simulations were run using the commercial software ANSYS Workbench 15.0 with its packaged Computational Fluid Dynamics (CFD) solver (Fluent 15.0) of Reynold's Averaged Navier-Stokes (RANS) using an unstructured mesh with $0.65 \cdot 10^6$ elements in average covering semispan of the computed baseline wing as shown in Fig. 2. Value of y+ is chosen to be less than five guaranteeing proper flow phenomena modelling at the boundary layer (Panagiotou *et al.* 2017). Mesh sensitivity checks showed stable convergence at various successive runs. Complicated mesh refining procedures and fluid domain structuring can definitely enhance the accuracy and resolution of the extractable solutions though at the expense of financial and operational resources, which ought to be considerably minimized during initial conceptual research stages (Okonkwo *et al.* 2016 and Panagiotou *et al.* 2017).

To enhance the confidence in CFD results two turbulence models, i.e., Spalart-Allmaras (S-A) and transition Shear Stress Turbulence (SST), were considered in the simulation for accuracy comparison. Both analysis were run in pressure-based, steady flow settings and solved using pressure-velocity coupling along with Least Squares Cell Based gradient and QUICK for remaining convection-diffusion equations within the discretization scheme settings. Turbulence model S-A is chosen to be vorticity-based while boundary conditions are given according to wing geometrical data in (Higgins *et al.* 1928) to satisfy Re = 500000. Hence, inflow speed equals 36.58 m/s that is equivalent to M = 0.106. Turbulence Intensity and viscosity ratio inputs are 1% and 0.2 to satisfy real flight conditions (Panagiotou *et al.* 2017). In Figs. 3 and 4 computation results are demonstrated for $-4° \leq \alpha \leq 24°$.

Good agreement with the experimental data is established along the α-span till $\alpha < 22°$ with

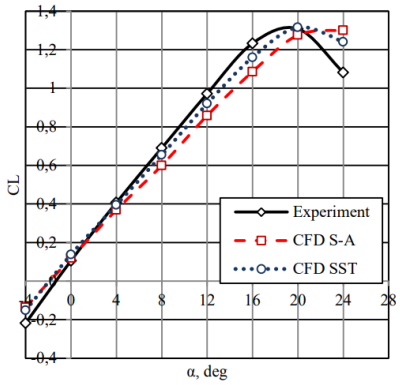

Fig. 3 Lift coefficient versus angle of attack of NACA-M6

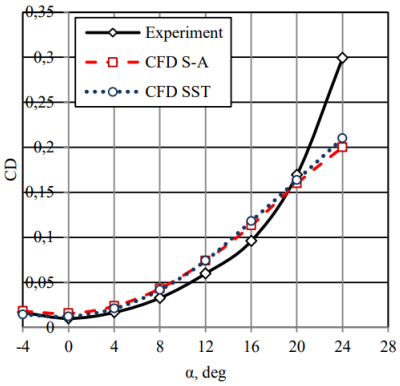

Fig. 4 Drag coefficient versus angle for attack of NACA-M6

accurate prediction of separation point in the case of SST model based simulation. Transition SST turbulence model records 95% precision within -4°< α < 22°, however as shown in Fig. 3, turbulence mode S-A produces quite approximate outputs at small α. Consequently, further analysis of BWB configurations adopts SST model due to its reliability and accuracy in predicting flow structure. Significant accuracy oscillations emerge while estimating wake turbulence and flow separation effects when exceeding stall values of α. This penalty characterizes all RANS models, where flow separation from smooth surfaces becomes exaggerated under the influence of adverse pressure gradients emergent at large α (Menter, 1992). More importantly, differences in the considered boundary conditions and Re values between the test in (Higgins *et al.* 1928) and present simulations might contribute in the ostensible accuracy reduction. For fair assessment similar testing and simulation conditions must be provided, which is a procedure that usually follows a successful conceptual design phase. Thus, further focus is given to aerodynamic performance at low turbulence α for their more distinctive credible and reliable results.

3. Results and discussion

This section summarizes and discuses results collected from a series of simulations for α = -4°… 22° with an interval of Δα = 4° for the chosen BWB models shown in Fig. 1 under the same

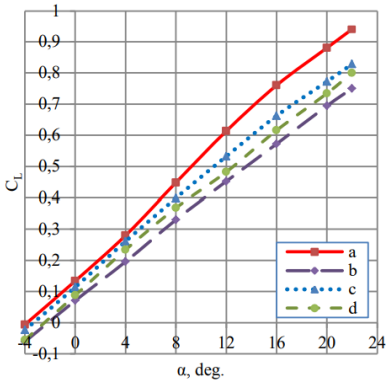

Fig. 5 Lift coefficient versus angle of attack for every BWB configuration

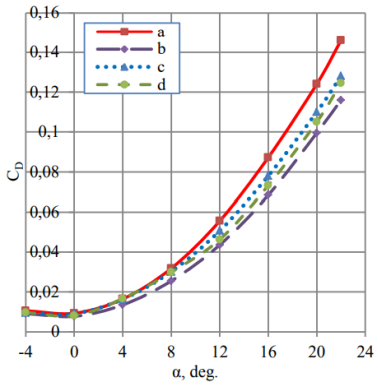

Fig. 6 Drag coefficient versus angle of attack for every BWB configuration

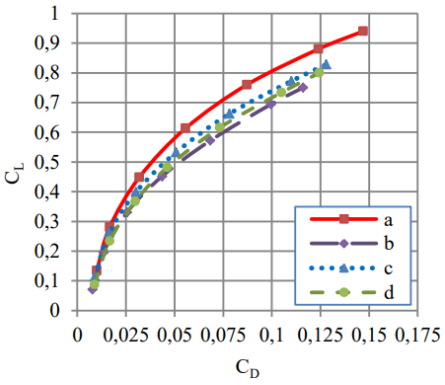

Fig. 7 Polar graph of the investigated BWB configurations

boundary conditions used for validating NACA-M6 computation. Root chord length is considered as the mean aerodynamic chord (MAC). In general, the following results outline the governing flow dynamics at low flight speeds u_i for every model indexed as i=a, b, c or d with respect to the chosen Re and calculated according to $u_i = \mu Re/l_i$: (a) = 25.2 m/s; (b) = 18.9 m/s; (c) = 19.9 m/s; (d) = 19.5 m/s calculated for MAC, where μ stands for the kinematic viscosity of the air at the

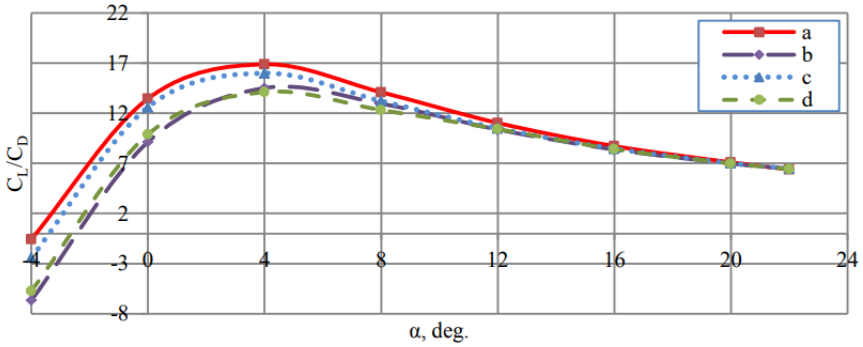

Fig. 8 Aerodynamic efficiency (C_L/C_D) versus angle of attack

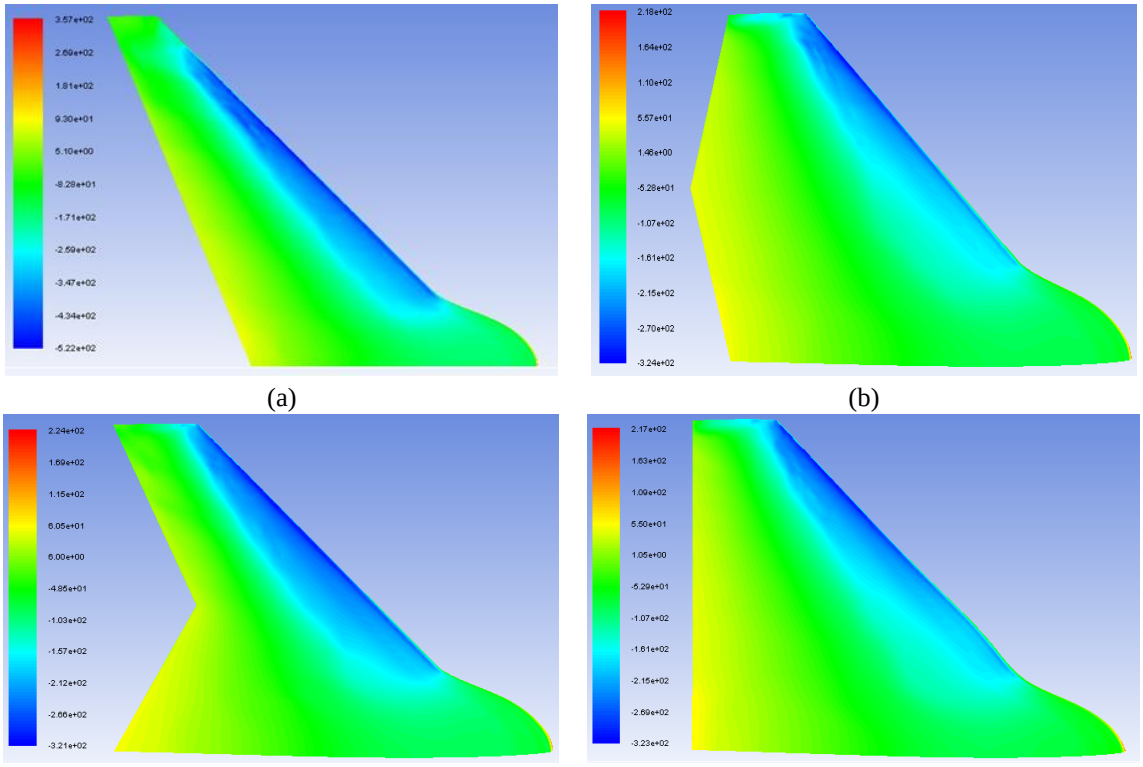

(a) (b)

(c) (d)

Fig. 9 Static pressure contour for every BWB configuration at α=22°

specified conditions and l_i denotes the root chord length of each model i.

In cruise flight mode, i.e., at α = 0°, (a) and (c) configurations share similar aerodynamic characteristics that exceed (b) and (d) in terms of the total lift coefficient (C_L) as shown in Fig. 5. In the case of drag forces similar results are seen in Fig. 6, where pressure drag makes the major contribution to drag coefficients (C_D) since wetted area and airfoil section are preserved for all configurations. Meanwhile, in the current flow regime designs (b, c, and d) incur less induced drag effects as a result of the insignificant differences in aspect ratio (AR) and taper (λ) than

configuration (a). It is worth noting that configuration (c) is similar to the tested one in (Patel M. *et al.* 2007), thus it is showing some degree of aerodynamic resemblance at pre-stalling flow regimes.

The notable improved aerodynamic performance of configuration (a) fundamentally stems from its relative high AR and λ compared to other BWB configurations due to high trailing edge sweepback, see Table 1. For configuration (c) analogical effect is rather attributed to the comparatively compound effects of high λ and AR featuring a reduction of induced drag (Zhang, P. *et al.* 2009). Delta-shaped BWB configuration (d) and its parallel with variable positive trailing edge sweep (b) aerodynamically resemble each other, although configuration (d) shows some insignificant increment within this flight mode. Plotted polar on Fig. 7 describes the function $C_{L\alpha}/C_{D\alpha}$ for every configuration, which again confirms the aerodynamic advantage of configurations (a and c) as ones with the maximum C_{D0}/C_{L0}, where C_{D0} and C_{L0} denote values of the related aerodynamic coefficients at $\alpha = 0°$.

Obvious divergence of aerodynamic characteristics occurs at non-horizontal flight modes. As noticed, high AR and low λ values of configuration (a) contribute to its superior performance in the range of $\alpha = 2 – 22°$ as shown in Fig. 8 for aerodynamic efficiency (K) per flow regime. Considering the fact that the same airfoil section was used for all investigated BWB configurations it is expected to observe $K_{max} = (C_L/C_D)_{max}$ at $\alpha = 4°$. Configurations (a and c) attain the highest $K_{a.max} = 16.9$ and $K_{c.max} = 16$ thanks to the given trailing edge geometry. Henceforth, the characteristic α for this particular flight mode will be called the efficient angle of attack (α_{ef}). Configurations (b and d) generally demonstrate an approximate performance at α_{ef} where $K_{b.max} = 14.5$ $K_{d.max} = 14.1$. The established maximum ratio of $(C_L/C_D)_{max}$ at α_{ef} as in configuration (a) indicates that the elliptic lift distribution yields the best relation between lift and drag forces in the case of BWB design with a good balance between AR and λ favoring constant trailing edge sweepback. This allows approaching the performance of efficient FW gliders.

Note that in Fig. 8 aerodynamic efficiency curves intersect at $\alpha = 22°$ revealing an identical K for all configurations at this flight mode. Accordingly, it is worthwhile to study flow properties at this particular α. In Fig. 9 spanwise surface static pressure contours for $\alpha = 22°$ are captured with eleven-scale legend for easier data presentation and comprehension. Taking into account the specific geometrical properties of each BWB configuration pressure gradient variation shows the largest difference of high and low pressure zones in the boundary layer and reveals the displacement of low pressure regain to the upper leading edge area of configuration (a) see Fig. 9(a). Certainly, this implies further favorable influences on the aerodynamic characteristics of the said BWB design. As expected, configuration (c) follows due to less centerbody surface involvement in lift generation. Because of the large centerbody surface leading to earlier turbulent flow instigation the remaining configurations (b and d) obtain smaller low pressure zone on the upper surface that eventually ends up contributing less local, i.e., area-averaged, lift coefficient to the total C_L. This highlights another aspect of the studied aerodynamic performance which relates to the comparative centerbody generated lift, whereas, for instance, it is found that configuration (a) produces about 1.5 times more lift than (d) at root chord section for $\alpha = 22°$; a difference that can be increased by mounting blades of the electric motor beyond the centerbody trailing edge of configuration (a) to help improving flow circulation and streamlining turbulent flow over the said zone especially at large α, see Fig. 0. Although such a propulsion system installation will increase stalling speed for all configurations, it seems that configuration (a) will benefit more advantage because of its less turbulence at trailing edge region when compared to (b, c, and d), see Fig. 10. On the other hand, if taking into account the separate design features and different blade

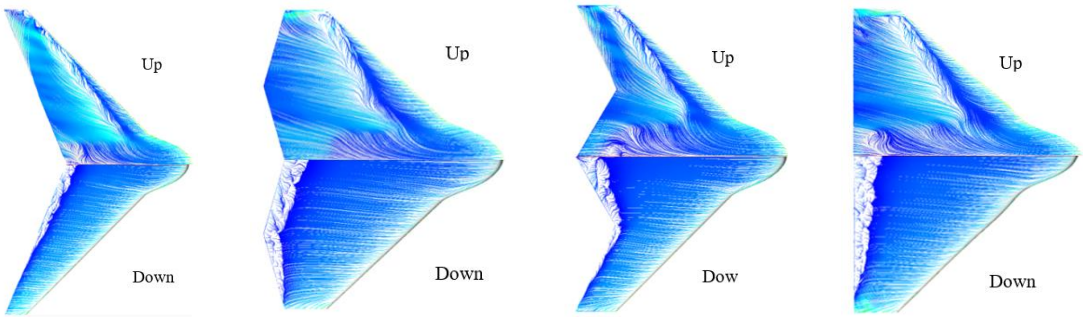

(a) (b) (c) (d)

Fig. 10 Flow patterns demostrated by surface streamlines for BWB configurations at α=22°

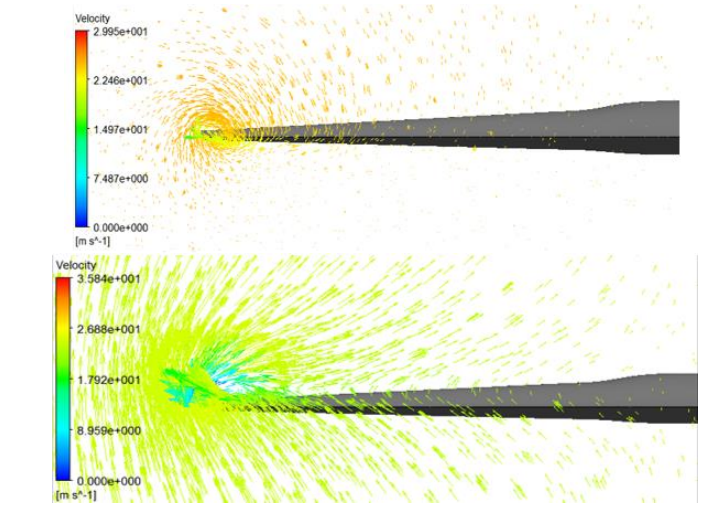

(a)

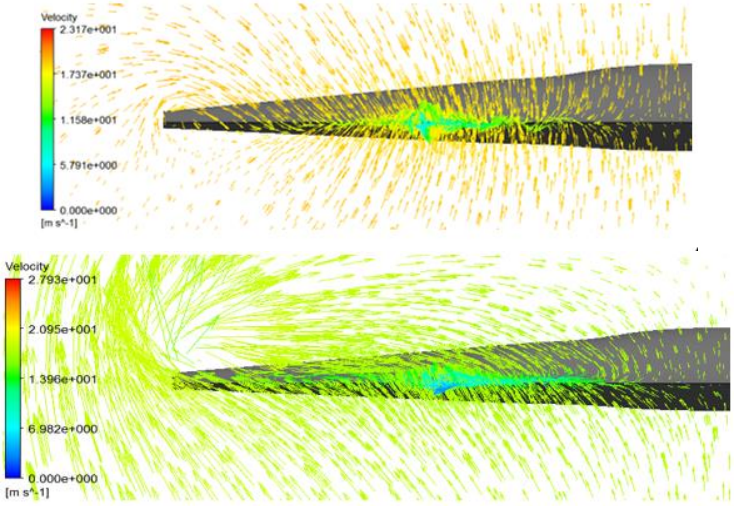

(b)

Fig. 11 Wingtip vortex velocity vector field at α = 0° (top) and 22° (bottom)

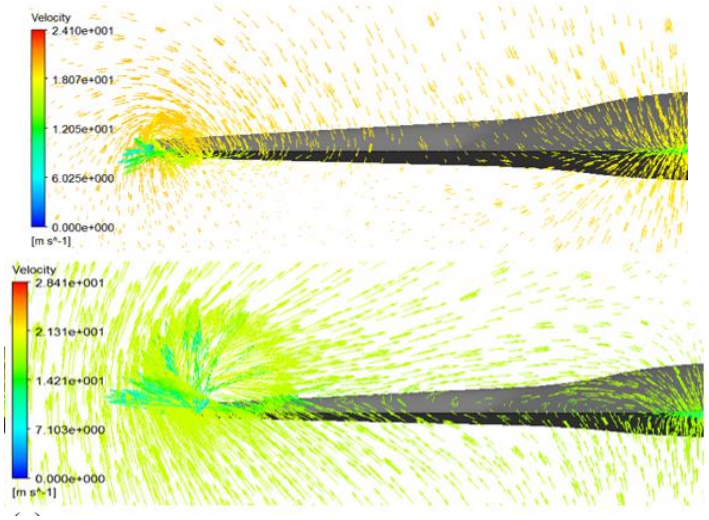

(c)

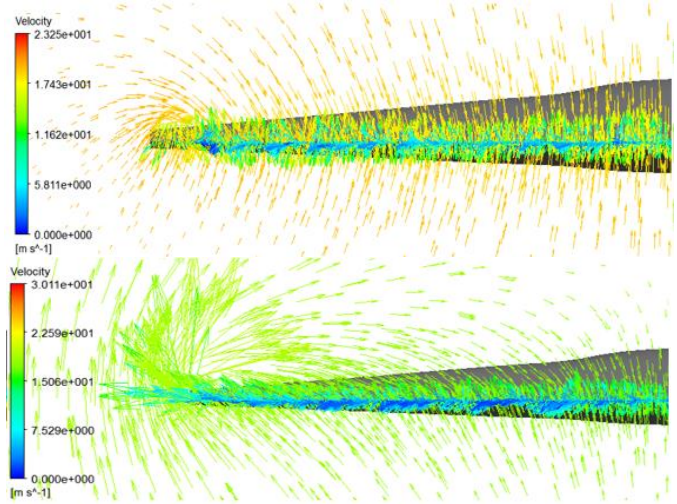

(d)

Fig. 11 Continued

diameters one should note that sometimes configurations (c and d) may provide easier mounting and more options for blade dimensions, for instance, a long rotor shaft may not be required. Thus, a relevant gain in overall propulsion system weight and torque can be attained.

One of the aerodynamic consequences associated with increasing trailing edge sweep is that $\lambda \rightarrow 0$. Its manifest effect shows up in the notable evolution of boundary layer spanwise flow which intensifies wingtip vortices. As shown in Fig. 10, boundary layer flow drift at $\alpha = 22°$ is observable by the representation of upper and lower surface streamlines. Configuration (a) has the smallest λ, therefore, it incurs the most intense wingtip vortices along the investigated range of α as they concentrate in furthest stagnation point on the trailing edge section. In the presence of more than one trailing edge stagnation point those vortices suffer kinetic energy dispersion enabling

some vorticity reduction at wingtip area. This is clearly evident on configurations (c, b, and d) when a tangential vector field of 4000 points wingtip vortices velocity evolving at $\alpha = 0°$ and 22° is projected on a normal plane intersecting with wingtip airfoil section trailing edge at $x/c = 1$, where x is the position of measurement point along the chord of definite length c, see Fig. 11. In the case of configuration (b) projection plane is attached to the trailing edge farthest point to easily capture potential multiple vortices. Note that configuration (d) has the most intense spanwise vortex field at zero α which explains its lower aerodynamic performance at this flight mode. On the other hand, variant trailing edge sweep of configuration (b) forms more than one separation point that results in more eddies and concentrated vortices. In Fig. 11 this configuration performs effective dispersion of trailing edge vortices comparatively achieving the least vortex velocity magnitudes. Referring to Fig. 10 another aspect to be highlighted is that both configurations (b and d) have the longest root sections. This geometrical property influences faster boundary layer transition and adverse pressure gradients generation and propagation along the trailing edge region. At small α, this creates approximate flow field velocities as seen in configurations (b and d) according to Fig.11. However, as α grows up most of the flow around trailing edge central region separates due to boundary layer detachment which increases pressure drag and consequently degrades the aerodynamic characteristics of all configurations to a similar performance at $\alpha = 22°$.

From the perspective of conceptual aerodynamic design, one implication to be indicated is the obvious relation between the improvement of aerodynamic performance and the constant trailing edge sweepback that directly generates bigger AR and smaller λ. Yet an interesting privilege of inconstant trailing edge sweep is its contribution to wingtip vortices scattering from various points as in configurations (b and c) or along the trailing edge span as in configuration (d). However, this phenomenon deteriorates flow circulation at the said locations on the wing planform as α increases leading to less K. Additional important note is that K implies better takeoff and landing performance for designs (a and c). This means shorter takeoff and landing field distance requirement or less catapulting power for UAVs with launching platforms. Thus, for vertical takeoff and landing UAVs this represents a secondary advantage. Another implication of the highlighted results may be the justification of why derived designs from configurations (c) are widely preferred for modern BWB combat and high maneuverability UAVs such as RQ-170 Sentinel, Northrop Grumman X-47B, and Boeing MQ-25 Stingray, and etc. It is attributed to the fact that it develops approximate K to configuration (a) and low magnitude of wingtip vortices compared to configurations (b and d) resulting in a better effectiveness of elevons during near stalling α and steep maneuvers. Moreover, it has larger centerbody volume than configuration (a) enabling more payload and onboard systems, devices, and elements distribution inside fuselage section. Additional advantage that is extremely favored in military subsonic UAVs is that configuration (c) and its derivatives have less radar cross-section due to smaller absolute size of the airframe. However, due to relatively shorter arm of the rolling and yawing moments created by elevons their span is designed wider imposing more trim drag penalty because of the increased area.

Configuration (a) achieves the highest K at positive $\alpha < 22°$ indicating appropriate aerodynamic performance for UAV mission profile that requires lower cruise speed but higher altitude and further flight ranges. However, note that this configuration has the smallest centerbody volume.

Due to the highest K configuration (a) develops the strongest spanwise structural loading, bending and torque, requiring stiffer and heavier structure. This reveals the additional comparative advantage of configuration (c) that shows up in its lower wing loading due to smaller AR. In

result, higher maneuverability, faster flight speeds, and lighter airframe. The same is applicable to configurations (b and d) but taking into consideration the easier design process and manufacturing procedure of configuration (d) compared to designs (c and b).

The aforementioned detailed description applies to UAVs without supplementary airframe parts such as motor nacelle and/or case, antenna envelop, or additional aerodynamic surfaces akin to wingtips and vertical stabilizers. In general, their attachment to airfoil-shaped sections of the chosen designs will deteriorate in one way or another overall aerodynamic performance, for which a comprehensive aerodynamic analysis should be developed.

4. Conclusions

Scarcity of comparative studies on the potential effect of trailing edge shape on the aerodynamic performance of low-speed small-size BWB configurations motivated this computational study to investigate four BWB configurations with different trailing edge geometries. Generic information for small-size BWB UAV designers is produced so as to facilitate decision making process during conceptual design phase. Detailed results justify the modern trend in favoring BWB designs derived from configurations (a and c) as they generate the highest aerodynamic efficiency at low angles of attack for the case when a standard airfoil is used for all BWB sections. In general, configuration (c) seems to have the optimum balance of aerodynamic performance and structural advantages. Positive sweep of the trailing edge as in configuration (b) seems to have an overall negative effect on the aerodynamic performance and structure weight although it weakens wingtip vortices.

More comprehensive studies covering correlation between trailing edge geometry and additional parameters such as dihedral angle and nose shapes at different Re ranges and weather conditions can enrich designer background and accelerate conceptualization process.

References

Ba Zuhair, M.A.M. (2018), *RU Patent No. 2,668,000*, BN, Federal Institute of Intellectual Property, Moscow, Russia.

Geiselhart, K.A., Daggett, D.L., Kawai, R. and Friedman, D. (2003), "Blended wing body systems studies: boundary layer ingestion inlets with active flow control", NASA/CR-2003-212670, NASA Reports.

Gursul, I. (2004), "Recent developments in delta wing aerodynamics", *Aeronaut. J.*, **108**(1087), 437-452. https://doi.org/10.1017/S0001924000000269.

Higgins, G.J. and Jacobs, E.N. (1928), "The effect of a flap and ailerons on the NACA M-6 airfoil section", NACA-TR-260, NASA Reports.

Kawai, R.T., Friedman, D.M. and Serrano, L. (2006), "Blended wing body (BWB) boundary layer ingestion (BLI) inlet configuration and system studies", NASA/CR-2006-214534, NASA Reports.

Kroo, I. (2004), "Innovations in aeronautics", *Proceedings of the 42nd AIAA Aerospace Sciences Meeting and Exhibit*, Reno, Nevada, U.S.A., January.

Kuntawala, N., Hicken, J. and Zingg, D. (2011), "Preliminary aerodynamic shape optimization of a blended-wing-body aircraft configuration", *Proceedings of the 49th AIAA Aerospace Sciences Meeting Including the New Horizons Forum and Aerospace Exposition*, Orlando, Florida, U.S.A., January.

Lehmkuehler, K., Wong, K. and Verstraete, D. (2012), "Design and test of a UAV blended wing body configuration", *Proceedings of the 28th Congress of the International Council of the Aeronautical Sciences*, Brisbane, Australia, September.

Liebeck, R.H. (2004), "Design of the blended wing body subsonic transport", *J. Aircraft*, **41**(1), 10-25. https://doi.org/10.2514/1.9084.

Meheut, M., Arntz, A. and Carrier, G. (2012), "Aerodynamic shape optimizations of a blended wing body configuration for several wing planforms", *Proceedings of the 30th AIAA Applied Aerodynamics Conference*, New Orleans, Louisiana, U.S.A., June.

Menter, F.R. (1992), "Performance of popular turbulence model for attached and separated adverse pressure gradient flows", *AIAA J.*, **30**(8), 2066-2072. https://doi.org/10.2514/3.11180.

Okonkwo, P. and Smith, H. (2016), "Review of evolving trends in blended wing body aircraft design", *Prog. Aerosp. Sci.*, **82**, 1-23. https://doi.org/10.1016/j.paerosci.2015.12.002.

Panagiotou, P. and Yakinthos, K. (2017), "Parametric aerodynamic study of Blended-Wing-Body platforms at low subsonic speeds for UAV applications", *Proceedings of the 35th AIAA Applied Aerodynamics Conference*, Denver, Colorado, U.S.A., June.

Patel, M.P., Ng, T.T., Vasudevan, S., Corke, T.C. and He, C. (2007), "Plasma actuators for hingeless aerodynamic control of an unmanned air vehicle", *J. Aircraft*, **44**(4), 1264-1274. https://doi.org/10.2514/1.25368.

Qin, N., Vavalle, A., Le Moigne, A., Laban, M., Hackett, K. and Weinerfelt, P. (2004), "Aerodynamic considerations of blended wing body aircraft", *Prog. Aerosp. Sci.*, **40**(6), 321-343. https://doi.org/10.1016/j.paerosci.2004.08.001.

Shim, H. and Park, S.O. (2013), "Low-speed wind-tunnel test results of a BWB-UCAV model", *Procedia Eng.*, **67**, 50-58. https://doi.org/10.1016/j.proeng.2013.12.004.

Siouris, S. and Qin, N. (2007), "Study of the effects of wing sweep on the aerodynamic performance of a blended wing body aircraft", *Proc. Inst. Mech. Eng. Part G J. Aerosp. Eng.*, **221**(1), 47-55. https://doi.org/10.1243%2F09544100JAERO93.

Spalart, P.R. and Rumsey, C.L. (2007), "Effective inflow conditions for turbulence models in aerodynamic calculations", *AIAA J.*, **45**(10), 2544-2553. https://doi.org/10.2514/1.29373.

Vicroy, D. (2009), "Blended-wing-body low-speed flight dynamics: summary of ground tests and sample results", *Proceedings of the 47th AIAA Aerospace Sciences Meeting including the New Horizons Forum and Aerospace Exposition*, Orlando, Florida, U.S.A., January.

Voskuijl, M., La Rocca, G. and Dircken, F. (2008), "Controllability of blended wing body aircraft", *Proceedings of the 26th International Congress of the Aronautical Sciences, ICAS 2008, including the 8th AIAA Aviation Technology, Integration and Operations (AIO) Conference*, Anchorage, Alaska, September.

Wisnoe, W., Kuntjoro, W., Mohamad, F., Nasir, R.E.M., Reduan, N.F. and Ali, Z. (2010), "Experimental results analysis for UiTM BWB baseline-I and baseline-II UAV running at 0.1 mach number", *Int. J. Mech.*, **4**(2), 23-32.

Wisnoe, W., Nasir, R.E.M., Kuntjoro, W. and Mamat, A.M.I. (2009), "Wind tunnel experiments and CFD analysis of Blended Wing Body (BWB) Unmanned Aerial Vehicle (UAV) at mach 0.1 and mach 0.3", *Proceedings of the 13th International Conference on Aerospace Sciences & Aviation Technology*, Cairo, Egypt, May.

Wood, R. and Bauer, X. (2011), "Flying wings/flying fuselages", *Proceedings of the 39th Aerospace Sciences Meeting and Exhibit*, Reno, Nevada, U.S.A., January.

Zhang, P.F., Wang, J.J., Liu, Y. and Wu, Z. (2009), "Effect of taper ratio on aerodynamic performance of cropped nonslender Delta wings", *J. Aircraft*, **46**(1), 320-325. https://doi.org/10.2514/1.32130.